DOI: 10.24352/UB.OVGU-2017-046 TECHNISCHE MECHANIK, 37, 1, (2017), 1 – 17
submitted: June 28, 2016

Frequency Shifts in Natural Vibrations in Pantographic Metamaterials under Biaxial Tests

A. Battista, D. Del Vescovo, N. L. Rizzi, and E. Turco

In this paper a 2D continuum model, thought as the homogenized limit of a microstructured pantographic sheet, is studied. The microstructure is characterized by two families of parallel fibers, whose deformation measures account for bending, elongation and relative rotation of the fibers. The deformation energy density of the homogenized model depends on both first and second gradients of the displacement. Modal analysis is performed in order to assess the peculiarities of the dynamic behavior of higher gradient models, and in particular the difference, with respect to classical laminae, in the dependence of the eigenfrequencies on the stiffness.

1 Introduction

Pantographic fabrics are a class of metamaterials in which two (or more) families of parallel fibers (with non negligible bending stiffness) interact by means of ideal hinges or rotational springs. The word *metamaterials* is used in the literature to emphasize the fact that they exhibit properties that are not found in natural materials (see e.g. Del Vescovo and Giorgio (2014); dell'Isola et al. (2015c)). A detailed theoretical description of these models is given in dell'Isola et al. (2016c,b); Placidi et al. (2016); dell'Isola et al. (2016d), while for experimental and numerical results the reader is referred respectively to Harrison (2016); dell'Isola et al. (2015a) and Scerrato et al. (2016c,b); Giorgio et al. (2016); Madeo et al. (2015). These materials have a very advantageous strength/weight ratio and a particularly safe behavior in fracture. Indeed, the failure region is rather localized and very well predictable, and moreover the structure keeps resisting for long beyond the beginning of the failure of the fibers (see dell'Isola et al. (2015a); Turco et al. (2016)). The mechanical behavior of such materials is therefore of interest in several areas of engineering, e. g. in biomechanics, aeronautic or aerospace industry and acoustic filters designing. A suitably complete and consistent theoretical treatment of these materials requires the development of material models in which the deformation energy depends on the second gradient of the displacement; the theory of higher gradient continua is by now a well developed chapter in continuum mechanics; the interested reader can see Germain (1973); Mindlin (1964) as classical sources, dell'Isola et al. (2009, 2011, 2016e) for the generalization of standard concept of elasticity to second gradient continua and dell'Isola et al. (2015b) for a review of results on the equivalence of energy and balance formulations on higher order continua.

One of the advantages of using second-gradient models is related to their very limited computational cost when compared to the numerical simulation in 3D of the detailed geometry of the microstructure Cuomo et al. (2016); dell'Isola et al. (2016a), since a second gradient homogenized model only captures the relevant average characteristics of the micro-model. Another advantage is linked to the possibility of describing the effect of point forces, which clearly can play a relevant role in case of fabrics, namely when a single fiber is stretched. Finally, second gradient models allow the description of the onset of boundary layers in the deformation, a behavior which is indeed observed even in standard bias extension tests Ferretti et al. (2014).

We want to remark that the justification of the second gradient homogenized limit of the pantographic fabric by means of rigorous mathematical arguments is beyond the scope of the present paper. However, rigorous results in this direction (although not immediately applicable to the case at hand) are already available for either 1D (Carcaterra et al. (2015)), 2D (Alibert and Della Corte (2015)) and 3D (Pideri and Seppecher (1997)) systems.

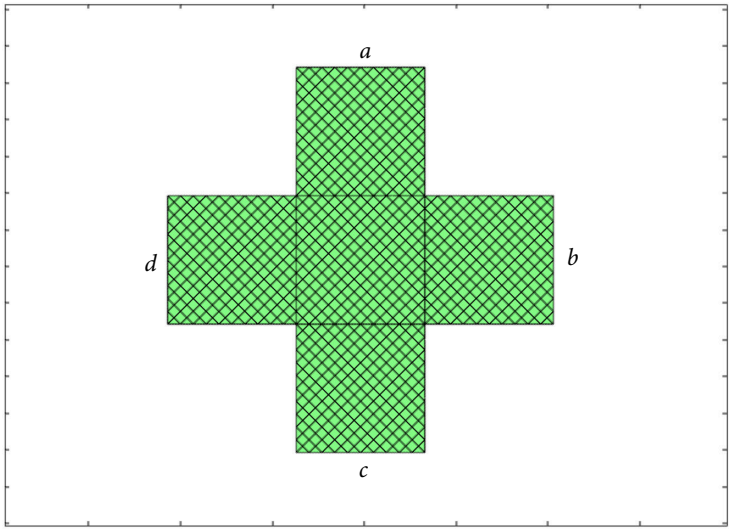

Figure 1: The reference configuration of the pantographic sample occupying the domain D.

2 In-plane Kinematics in Pantographic Metamaterials

Let us consider a cross-shaped plane surface occupying the subset D of $\mathbb{R}^2$ defined by:

$$D := \left\{ \left[-\frac{L}{2}, \frac{L}{2} \right] \times \left[-\frac{L}{6}, \frac{L}{6} \right] \bigcup \left[-\frac{L}{6}, \frac{L}{6} \right] \times \left[-\frac{L}{2}, \frac{L}{2} \right] \right\} \tag{1}$$

The domain D corresponds to the (unstressed) reference configuration of a 2D continuum model representing the homogenized limit of a pantographic microstructured sheet. The microstructure here considered consists of two sets, S_1 and S_2, of parallel fibers, modeled as extensible Euler beams, inclined at 45 degrees with respect to the sides of the domain D and mutually orthogonal. The domain, with the relative arrangement of the fibers, is graphically represented in Fig. 1.

The choice of this particular shape is due to the fact that it is commonly used for biaxial tests addressed at estimating shear stress on engineering fabrics, and in particular the coupling between shear resistance and in-plane tension (see Harrison and Potluri (2009); Harrison (2012); Harrison et al. (2012)).

The placement of the sample is described by a suitably regular, bijective function $\boldsymbol{\chi}$:

$$\boldsymbol{\chi} : \boldsymbol{X} \in D \rightarrow \boldsymbol{\chi}(\boldsymbol{X}) \in \mathcal{E}^2 \tag{2}$$

where $\mathcal{E}^2$ is the standard affine Euclidean plane. Besides, the displacement is $\boldsymbol{u}(\boldsymbol{X}) := \boldsymbol{\chi}(\boldsymbol{X}) - \boldsymbol{X}$. Here we limit ourselves to a brief, although self-consistent, description (for a complete justification of the model see the literature cited in the previous section).

In what follows, $\mathbf{D}_1$ and $\mathbf{D}_2$ are the unit vectors of the canonical basis in $\mathbb{R}^2$. Let us assume that the fibers are oriented along $\mathbf{D}_1$ and $\mathbf{D}_2$; the deformation measures that we consider are the following:

- a strain measure, due to the *stretch of fibers*

$$\varepsilon_\alpha = \|\boldsymbol{F}\mathbf{D}_\alpha\| - 1, \tag{3}$$

  where $\boldsymbol{F}$ is the deformation gradient $\boldsymbol{F} := \nabla\boldsymbol{\chi}$ and the index α runs over $\{1, 2\}$

- a bending measure, due to the *curvature of the fibers*

$$\kappa_\alpha = \|\boldsymbol{c}_\alpha - (\boldsymbol{c}_\alpha \cdot \boldsymbol{e}_\alpha)\, \boldsymbol{e}_\alpha\| = \|(\boldsymbol{I} - \boldsymbol{e}_\alpha \otimes \boldsymbol{e}_\alpha)\, \boldsymbol{c}_\alpha\|\,, \tag{4}$$

where κ_α is the curvature of the fiber belonging to the family S_α multiplied by $\|\boldsymbol{F}\mathbf{D}_\alpha\|$, $\boldsymbol{I}$ is the identity matrix, and $\boldsymbol{e}_\alpha$ and $\boldsymbol{c}_\alpha$ are defined as follows:

$$\boldsymbol{e}_\alpha := \frac{\boldsymbol{F}\mathbf{D}_\alpha}{\|\boldsymbol{F}\mathbf{D}_\alpha\|}, \quad \boldsymbol{c}_\alpha := \frac{\nabla \boldsymbol{F}|\mathbf{D}_\alpha \otimes \mathbf{D}_\alpha}{\|\boldsymbol{F}\mathbf{D}_\alpha\|} \tag{5}$$

- a shear measure, due to the *shear angle* between the fibers of the two families, i.e. the difference $\frac{pi}{2} - \theta$, where θ is the angle between the fibers in the deformed configuration. The angle γ is therefore defined as:

$$\gamma := \arcsin(\boldsymbol{e}_1 \cdot \boldsymbol{e}_2). \tag{6}$$

We have therefore the following surface deformation energy density (dell'Isola et al. (2016d)):

$$\Psi(\varepsilon_\alpha, \kappa_\alpha, \gamma) = \sum_\alpha \left(\frac{1}{2} K_I \varepsilon_\alpha^2 + \frac{1}{2} K_{II} \kappa_\alpha^2\right) + \frac{1}{2} K_p \gamma^\beta \tag{7}$$

where K_I, K_{II} and K_p are respectively the stretching, bending and shear stiffness, and β is a scalar accounting for the material nonlinearity of the sample with respect to shear (the value for β used in the simulations was chosen in order to fit experimental data, see dell'Isola et al. (2016d)). Assuming for simplicity that inertial effects are only due to the displacement of the centroid of the fibers' cross-sections, we consider the following kinetic energy:

$$T(\dot{\boldsymbol{\chi}}) = \frac{1}{2} \varrho_{\mathcal{S}}\, \dot{\boldsymbol{\chi}} \cdot \dot{\boldsymbol{\chi}} \tag{8}$$

where $\varrho_{\mathcal{S}}$ is the surface mass density (assumed constant) and dot represents time differentiation.

We have, in conclusion, the Lagrangian $\mathcal{L} := \int_D (T - \Psi) \mathrm{d}\boldsymbol{X}$, and the action $\mathcal{A} := \int_{t_0}^{t_F} \mathcal{L} \mathrm{d}t$.

3 Numerical Results

We first considered the static problem of a sample, having the fibers oriented along $\mathbf{D}_1$ and $\mathbf{D}_2$, subject to a tensile biaxial test. In this test, a prescribed uniform displacement is imposed to the four (external) short sides a, b, c and d of the sample. The four displacements are orthogonal to the side which they are applied to, and all have the same modulus U. We numerically solve this problem, for different values U_k, $k = 1, 2, 3$ of the modulus of the prescribed displacement, including all geometric and material nonlinearities. The solution is obtained by means of a standard Finite Element Method, with Hermite elements and cubic polynomials (as in Scerrato et al. (2016c); Giorgio (2016); more sophisticated formulations for Finite Element schemes, allowing higher regularity between the elements, can be useful in case of higher gradient models, as for instance Isogeometric Analysis, see Greco and Cuomo (2016, 2015); Cazzani et al. (2016b,a)). The force-displacement graph concerning one of the four short sides of the sample is plotted in Fig. 2. In the graph, the resultant force on the side is plotted versus the modulus of the imposed displacement.

The data used for the previous simulation, as well as all other simulations presented later, are shown in Table 1 (all values come from dell'Isola et al. (2016d)). The moduli of the three displacements U_1, U_2 and U_3 are respectively 0.1ℓ, 0.2ℓ and 0.4ℓ, where $\ell := \frac{L}{3} = 7$ cm.

Table 1: Data used in the numerical simulations of pantographic fabric.

L	K_I	K_{II}	K_p	β	$\varrho_{\mathcal{S}}$
21 cm	1.34×10^5 N/m	0.0192 N m	159 N/m	1.36	0.564 kg/m^2

The deformed equilibrium shapes corresponding to $k = 1, 2, 3$ are shown in Figs. 3, 4 and 5, left panels. We also considered an asymmetric test in which the displacement is imposed only to two opposite short sides, while the other two are clamped (i.e. have an imposed zero displacement). The relative deformed equilibrium shapes are

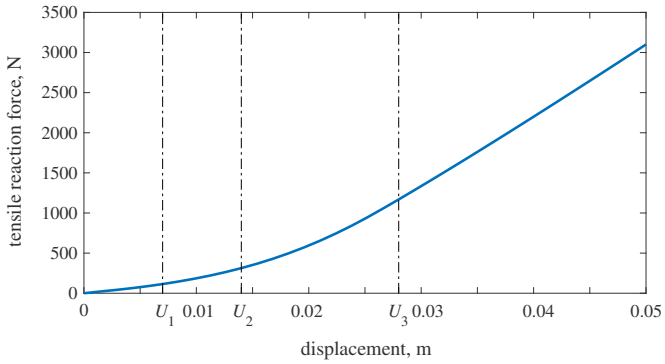

Figure 2: Force-displacement plot for a biaxial bias extension test

represented in Figs. 3, 4 and 5, right panels. In all cases, it is possible to observe that the square central area the deformation is an almost uniform pure shear.

Next we considered the linearized problem starting from the configurations C_k corresponding to the equilibrium shape with imposed displacements $\boldsymbol{U}_k$. Standard modal analysis is performed around these configurations.

In Figs. 6, 7 and 8 the first 12 mode shapes corresponding to $k = 1, 2, 3$ (i.e. modulus of the imposed displacement equal respectively to 0.1ℓ, 0.2ℓ and 0.4ℓ), in the case of symmetric biaxial test, are shown. In the picture, the deformation energy density of the mode shape is shown in color map, and only the harmonic perturbation is shown, i.e. the deformed shape is polished from prestress displacement. It is possible to observe that the mode shapes are significantly different for different values of the prestress. In particular, in the latter case boundary layers are not visible anymore, while the deformation energy of the mode shape is concentrated in proximity of the boundary of the sample. In Table 3 we show the values of the eigenfrequencies corresponding to these mode shapes for $k = 1, 2, 3$. While most of the eigenfrequencies show the usual monotonicity with respect to the imposed prestress (i.e. a larger prestress induces larger values of the eigenfrequency), modes 9 and 10 for the cases $k = 1$ and $k = 2$ show an inverse monotonicity between frequencies and displacement. A detailed analytical explanation of this phenomenon is far from trivial, and future investigations of mathematical nature will be addressed to it. However, it is possible to provide a simple qualitative argument that probably captures the crucial point behind it. Indeed, since the norm of $\boldsymbol{F}\mathbf{D}_\alpha$ appears at the denominator of $\boldsymbol{c}_\alpha$ (see eq. 5, right), it is clear that the deformation measures ε_α and κ_α are coupled in such a way that an increase in the strain deformation is connected to a decrease of the bending deformation (interesting results on the eigenfrequencies in case of prestress are studied in Altenbach et al. (2011); Eremeyev and Lebedev (2016)).

We can compare these results with analogous mode shapes for an orthotropic lamina having the same geometry and the same surface mass density. For that purpose, let us consider a classical lamina whose thickness is h and is governed by the following equations:

$$\Psi^L(E_{ij}) = \frac{1}{2} h\, \sigma_{ij} E_{ij} \tag{9}$$

where E_{ij} are the components of the strain tensor depending on the displacement field as follows

$$E_{ij} = \frac{1}{2}\left(\frac{\partial u_i}{\partial X_j} + \frac{\partial u_j}{\partial X_i} + \frac{\partial u_r}{\partial X_i}\frac{\partial u_r}{\partial X_j}\right) \tag{10}$$

σ_{ij} are the components of the stress tensor which can be evaluated by the following constitutive relationship

$$\begin{pmatrix}\sigma_{11}\\ \sigma_{22}\\ \sigma_{12}\end{pmatrix} = \begin{pmatrix}Q_{11} & Q_{12} & 0\\ Q_{12} & Q_{22} & 0\\ 0 & 0 & Q_{32}\end{pmatrix}\begin{pmatrix}E_{11}\\ E_{22}\\ E_{12}\end{pmatrix} \tag{11}$$

and the stiffness parameters are given by:

$$Q_{11} = \frac{Y_1}{1-\nu_{12}\nu_{21}}; \quad Q_{22} = \frac{Y_2}{1-\nu_{12}\nu_{21}}; \tag{12}$$

$$Q_{12} = \frac{Y_2\,\nu_{12}}{1-\nu_{12}\nu_{21}}; \quad Q_{32} = G_{12} \tag{13}$$

being Y_1 and Y_2 the Young moduli, ν_{12} and ν_{21} the Poisson ratios related to the orthotropic directions $\mathbf{D}_1$ and $\mathbf{D}_2$, respectively; while G_{12} is the shear modulus.The numerical values of these parameters used in the simulation for the lamina are shown in Table 2 (the values were chosen so as to have an approximate equivalence in the deformation energy with the considered external actions). The kinetic energy used in this case is the same as in Eq. (8).

We imposed to the lamina the same displacements prescribed to the pantographic fabric, and then performed modal analysis. The results are shown in Fig. 9 for a displacement having modulus 0.1ℓ. It is possible to observe that the mode shapes are completely different from the case of the pantographic fabric. Also, the eigenfrequency is here always an increasing function of the prestress for each mode shape.

Table 2: Data used in the numerical simulations of orthotropic lamina.

h	$Y_1 = Y_2$	G	$\nu_{12} = \nu_{21}$	ϱ_S
1.6 mm	1600×10^6 N/m^2	1.512×10^5 N/m^2	0.3	0.564 kg/m^2

Finally, we considered the pantographic fabric subject to an asymmetric extension test. We show in Figs. 10, 11 and 12 the first 12 mode shapes starting from equilibrium configurations shown in Figs. 3, 4 and 5, right panels. Again, the deformation energy density of the mode shape is shown in color map and only the harmonic perturbation is shown. In Table 5 we show the values of the eigenfrequencies corresponding to these mode shapes for $k = 1, 2, 3$. Here again a frequency shift, i.e. a decrease of the eigenfrequency in correspondence to an increase of the prestress, is observable in modes 9 and 10 comparing the case $k = 2$ and $k = 3$.

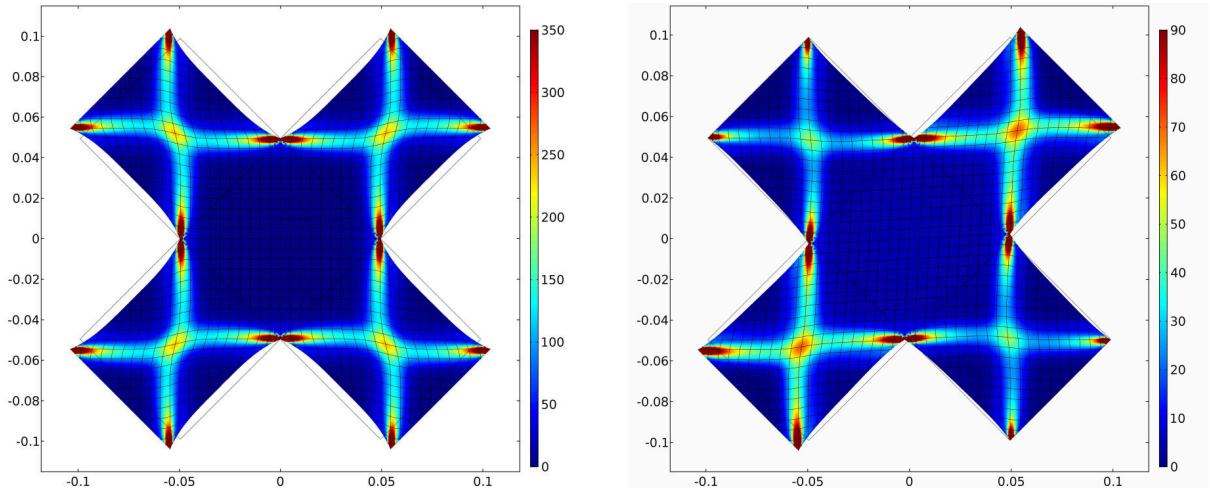

Figure 3: Reference and actual configuration of a symmetric and an asymmetric biaxial text ($U_1 = 0.1\ell$). The colours indicate the level of the deformation energy density Ψ.

Table 3: Case of symmetric biaxial test for the pantographic fabric: Mode frequencies, rad/s.

Mode #	$U_1 = 0.1\ell$	$U_2 = 0.2\ell$	$U_3 = 0.4\ell$
1	1751.8	2567.9	5112.7
2	1751.9	2568.1	5112.7
3	2983.9	3932.5	6244.8
4	3443.4	4550.1	8767.9
5	5064.6	6245.6	8767.9
6	5064.7	6246.3	9295.6
7	6688.9	6723.4	9673.9
8	6846.2	7080.1	9676.9
9	8113.8	7080.1	10419.7
10	8113.9	7536.6	10495.3
11	8123.1	8178.0	10495.3
12	8792.9	8434.0	10952.0

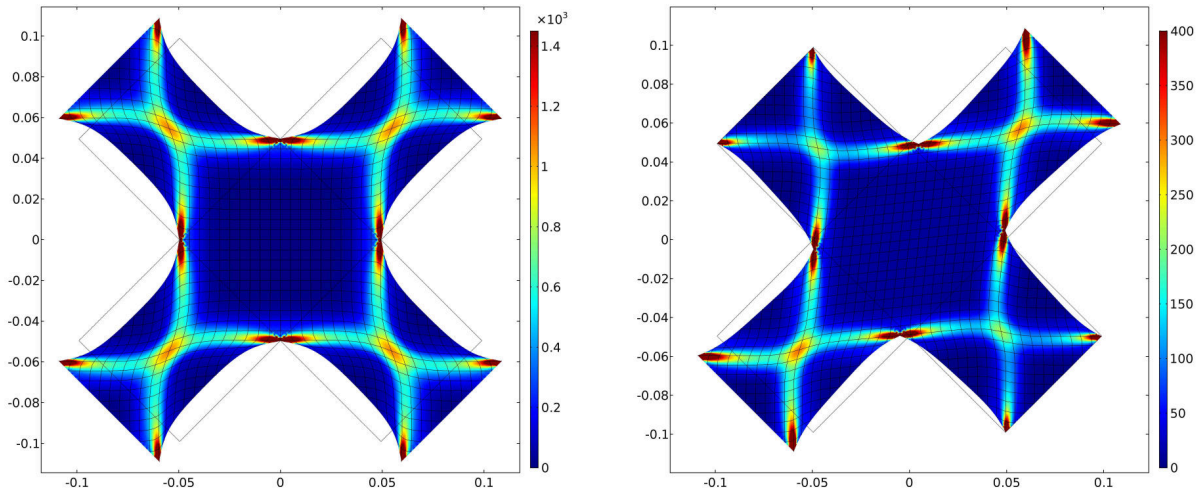

Figure 4: Reference and actual configuration of a symmetric and an asymmetric biaxial text ($U_2 = 0.2\ell$). The colours indicate the level of the deformation energy density Ψ.

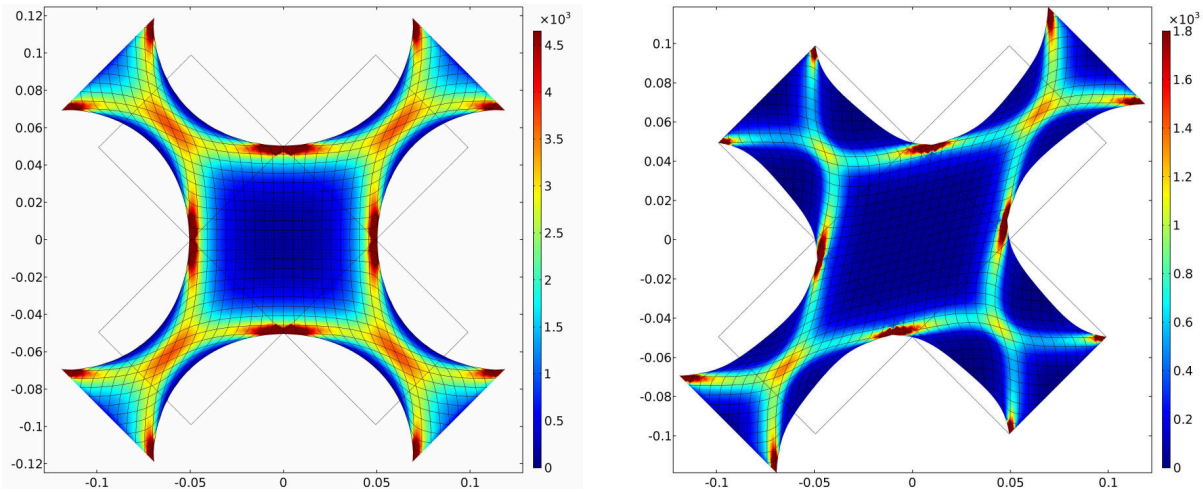

Figure 5: Reference and actual configuration of a symmetric and an asymmetric biaxial text ($U_3 = 0.4\ell$). The colours indicate the level of the deformation energy density Ψ.

Table 4: Case of symmetric biaxial test for the orthotropic lamina: Mode frequencies, rad/s.

Mode #	$U_1 = 0.1\ell$	$U_2 = 0.2\ell$	$U_3 = 0.4\ell$
1	1571.9	2734.5	5537.9
2	1571.9	2734.5	5537.9
3	2692.8	4380.2	7477.8
4	2866.8	4830.6	7945.8
5	4256.5	6885.8	9445.4
6	4256.5	6885.8	9473.9
7	5314.4	8397.8	9473.9
8	5618.7	8788.3	9589.8
9	6890.7	9497.9	10005.5
10	6890.7	9713.9	10005.5
11	7858.2	10135.0	11723.0
12	8161.0	10779.0	13223.0

Table 5: Case of asymmetric biaxial test for the pantographic fabric: Mode frequencies, rad/s.

Mode #	$U_1 = 0.1\ell$	$U_2 = 0.2\ell$	$U_3 = 0.4\ell$
1	1283.2	1595.1	2520.8
2	1290.2	1742.5	3235.2
3	2244.4	2765.1	4098.6
4	2381.6	3072.8	4615.5
5	3621.0	4497.9	6057.4
6	3704.2	4527.1	6160.9
7	4976.3	5853.1	6179.8
8	5094.6	6152.7	6453.9
9	6573.8	7417.7	6693.0
10	6647.2	7707.6	6854.1
11	8096.1	7753.0	8269.1
12	8121.8	8201.0	8394.7

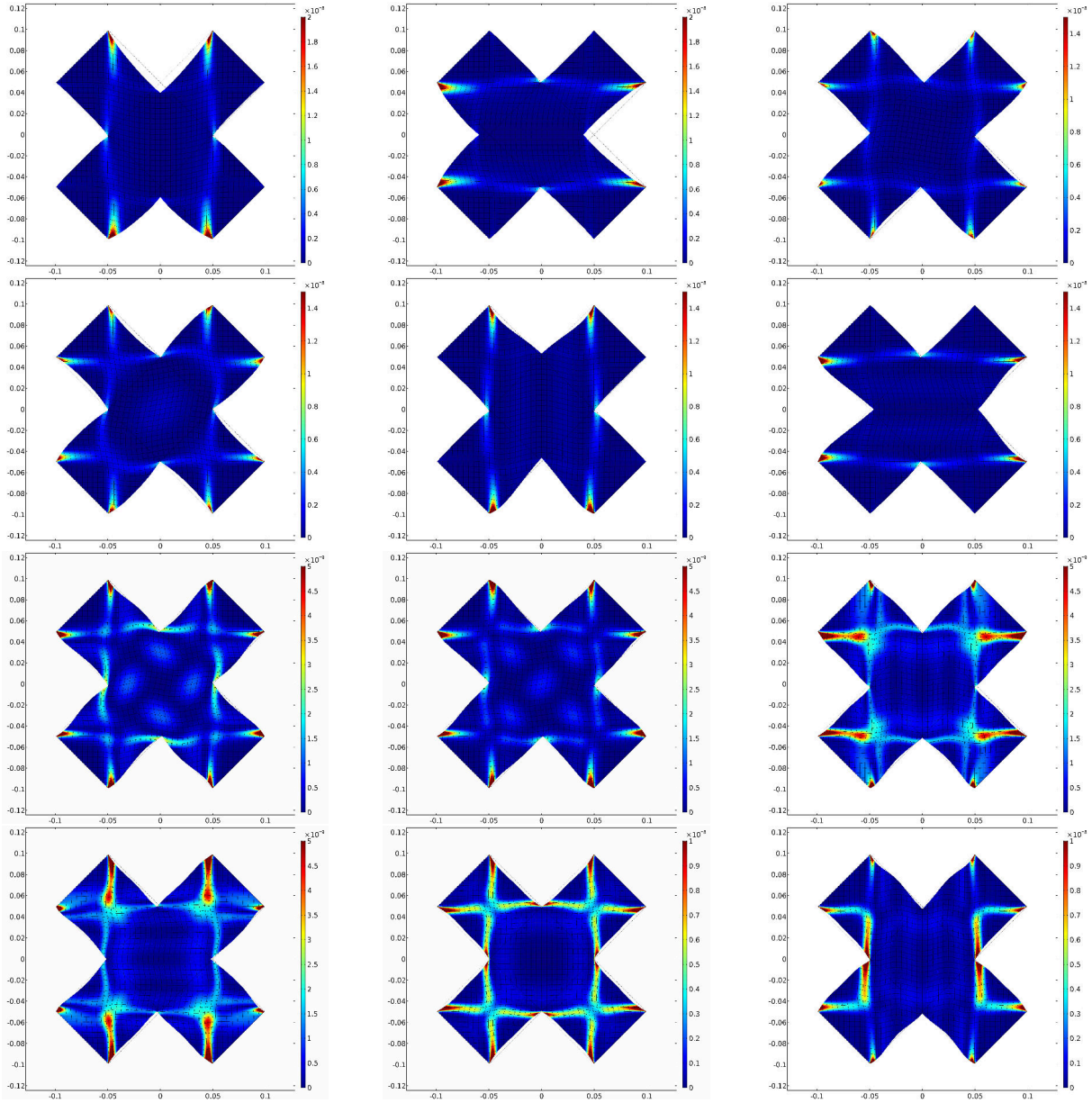

Figure 6: Mode shapes of a symmetric biaxial text for the pantographic fabric ($U_1 = 0.1\ell$).

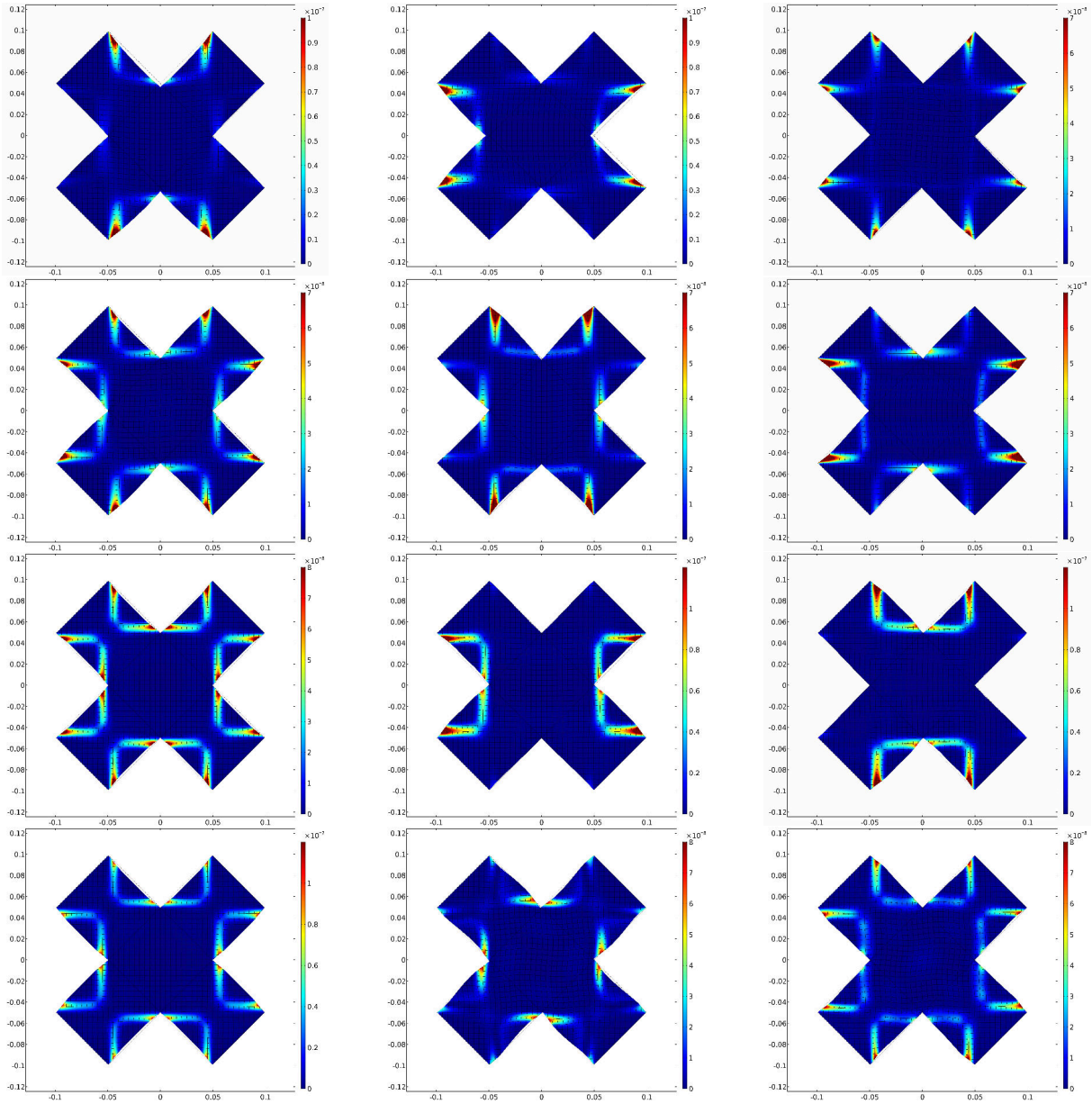

Figure 7: Mode shapes of a symmetric biaxial text for the pantographic fabric ($U_2 = 0.2\ell$).

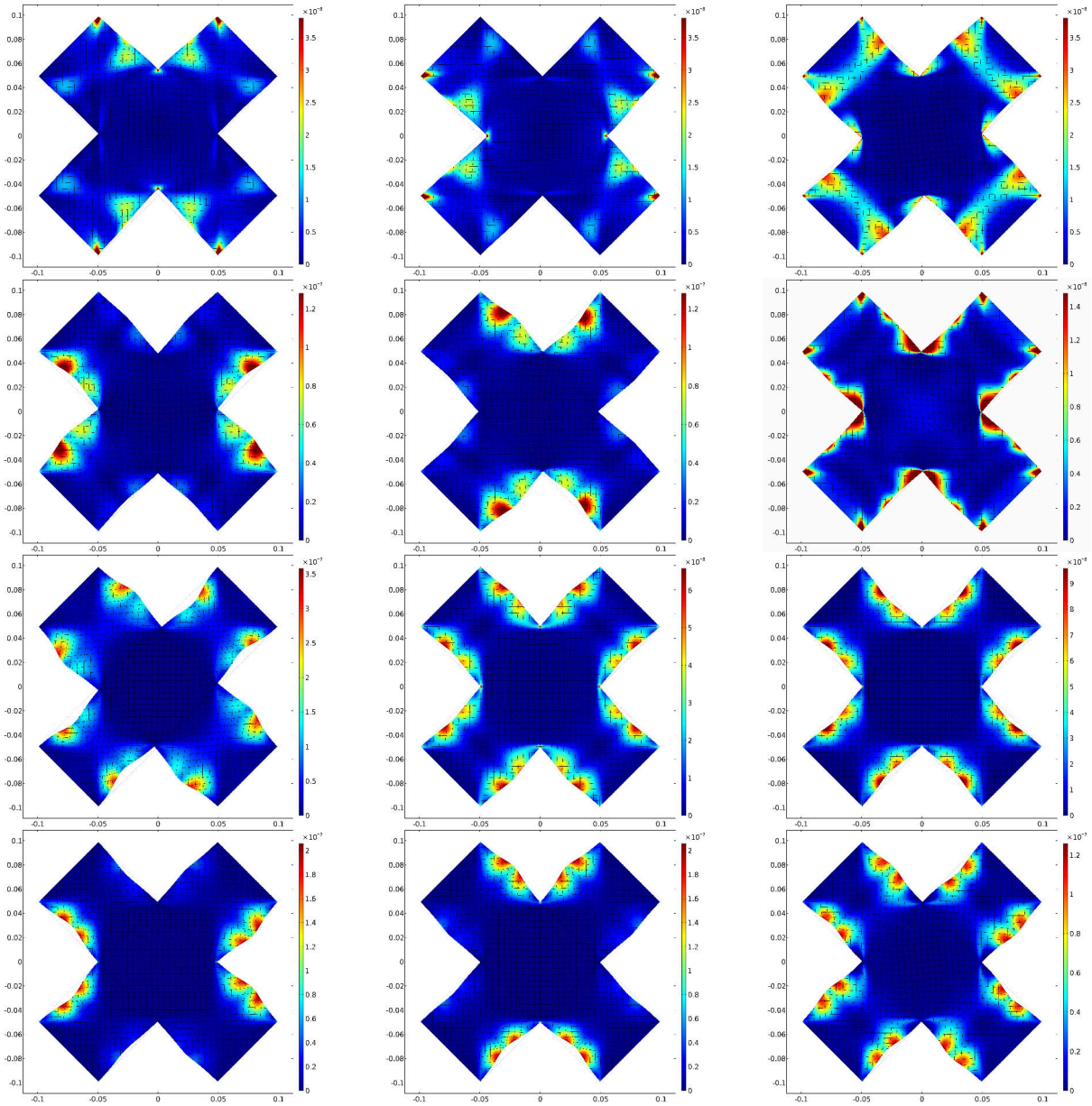

Figure 8: Mode shapes of a symmetric biaxial text for the pantographic fabric ($U_3 = 0.4\ell$).

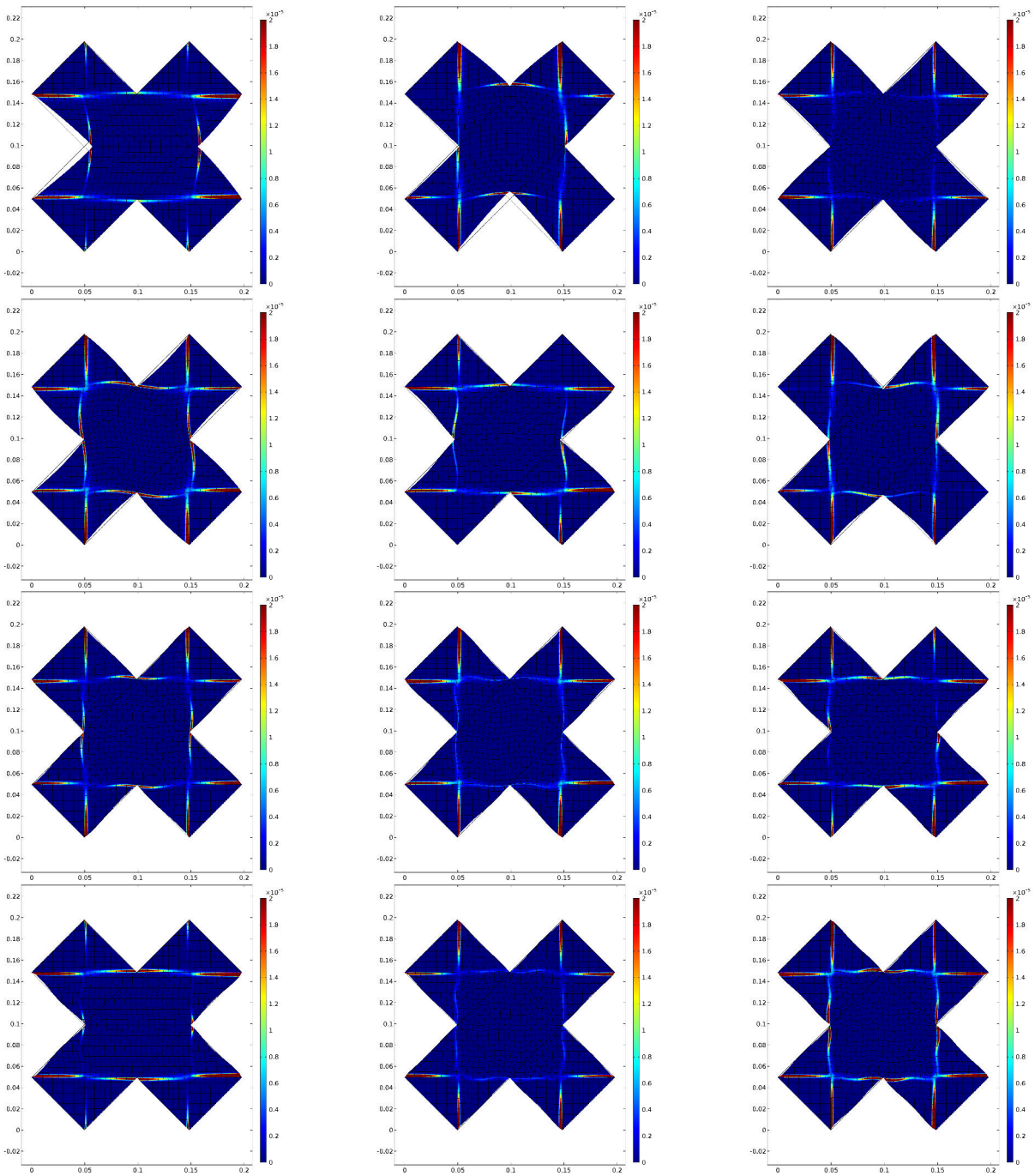

Figure 9: Mode shapes of a symmetric biaxial text for the orthotropic lamina ($U_1 = 0.1\ell$).

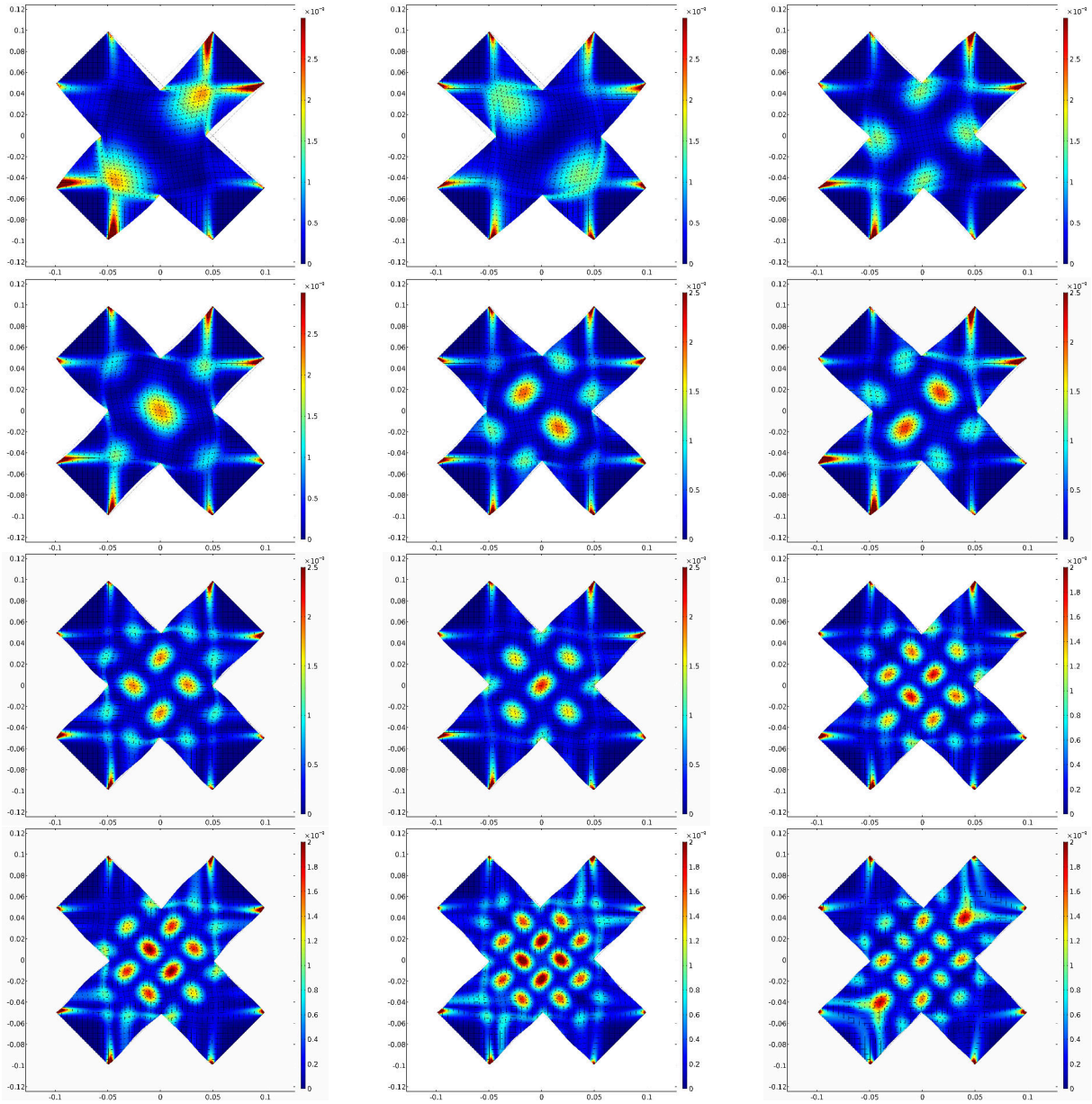

Figure 10: Mode shapes of an asymmetric biaxial text for the pantographic fabric ($U_1 = 0.1\ell$).

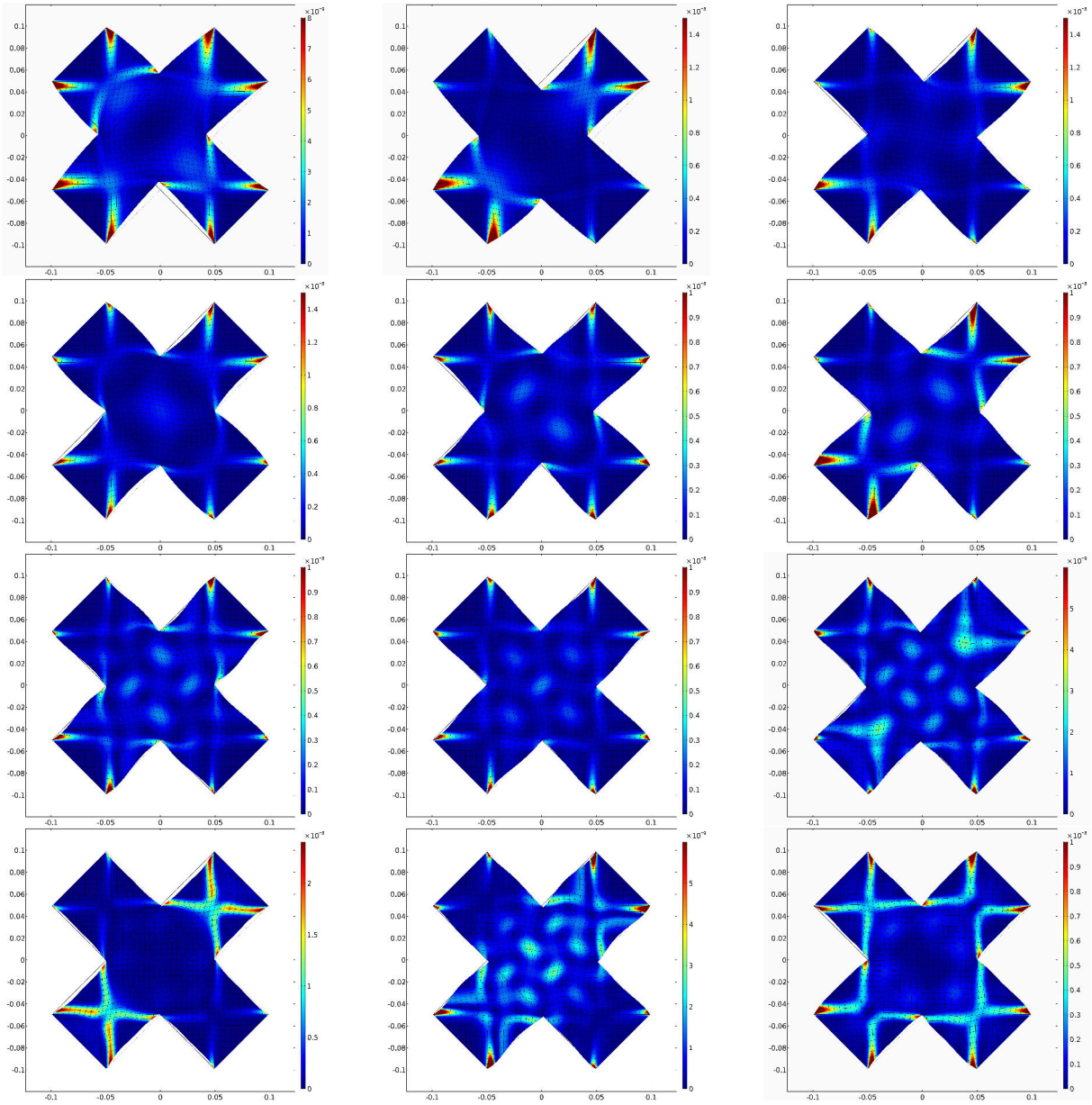

Figure 11: Mode shapes of an asymmetric biaxial text for the pantographic fabric ($U_2 = 0.2\ell$).

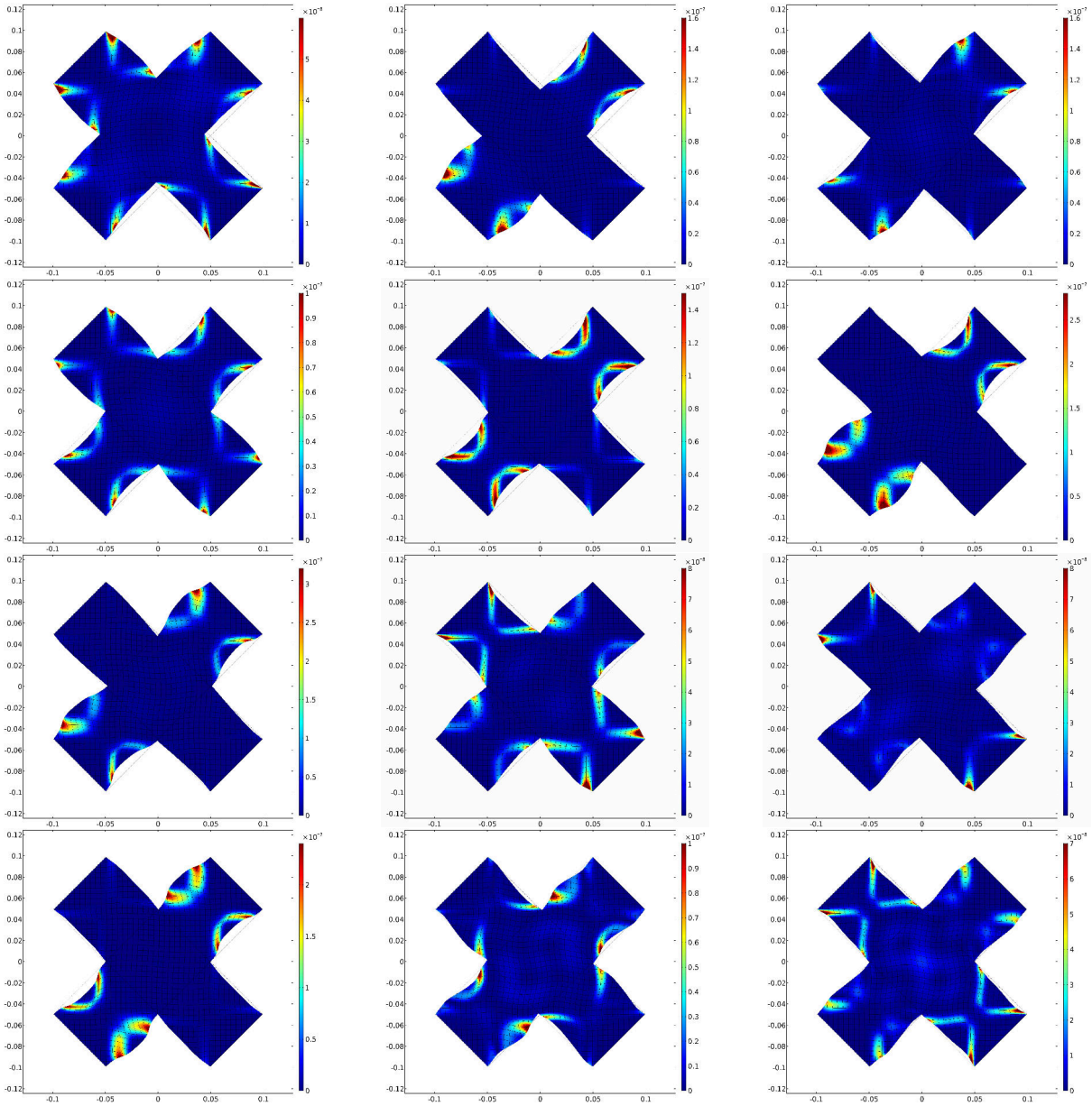

Figure 12: Mode shapes of an asymmetric biaxial text for the pantographic fabric ($U_3 = 0.4\ell$).

4 Conclusions

In this article, we performed a modal analysis on the homogenized limit of a pantographic fabric, modeled as a second gradient continuum. Mode shapes are analyzed starting from different equilibrium configurations, obtained solving a geometrically nonlinear static problem with imposed displacements. The mode shapes are compared with the ones obtained with an orthotropic lamina having the same geometry. The comparison shows that the mode shapes are significantly different in the two cases. In particular, it is shown an inverse eigenfrequency shift in the case of the pantographic fabric with respect to the lamina, i.e. in the former case the eigenfrequencies decrease in correspondence of an increase of the prestress for certain modes.

The results can be important for the understanding of the dynamic behavior of fabrics with pantographic microstructures and in particular for their employment in vibration control. As a perspective research direction, the coupling of the fibers of the pantographic fabric (or some of them) with piezoelectric and/or flexoelectric components (i.e. objects displaying a spontaneous electrical polarization induced by the second gradient of the displacement) can be effective for the realization of passive damping systems (see e.g. Giorgio et al. (2015); Maurini et al. (2004); Alessandroni et al. (2004); Enakoutsa et al. (2016); Shen et al. (2010)). In view of these potential applications, it can also be noted that Euler beam model for the description of the fibers may prove too restrictive to include the relevant characteristics of real-world pantographic fabrics, since the distance between nodes can be too small and/or the cross section of the fibers can undergo significant deformation. In this connection, suitably generalized models (see e.g. Luongo and Zulli (2013); Piccardo et al. (2014); Ranzi and Luongo (2011)) can be important to improve the predictability of the theory.

We finally observe that, having in mind vibration control problems, it would be interesting to take into account the dissipation possibly arising as a consequence of the contact of the fibers (Nadler and Steigmann (2003); Harrison et al. (2004)). In this respect, woven and non-woven fabrics will produce very different results, and the friction resulting from the relative displacement of the fibers could be modeled as Coulomb-type, or by means of more general friction models (e.g. stick-slip or smoothened Coulomb, as in Scerrato et al. (2014, 2015); Giorgio and Scerrato (2016); Scerrato et al. (2016a)).

References

Alessandroni, S.; Andreaus, U.; dell'Isola, F.; Porfiri, M.: Piezo-electromechanical (PEM) Kirchhoff–Love plates. *European Journal of Mechanics-A/Solids*, 23, 4, (2004), 689–702.

Alibert, J.-J.; Della Corte, A.: Second-gradient continua as homogenized limit of pantographic microstructured plates: a rigorous proof. *Zeitschrift für angewandte Mathematik und Physik*, 66, 5, (2015), 2855–2870.

Altenbach, H.; Eremeyev, V. A.; Lebedev, L. P.: On the spectrum and stiffness of an elastic body with surface stresses. *ZAMM-Zeitschrift für Angewandte Mathematik und Mechanik*, 91, 9, (2011), 699–710.

Carcaterra, A.; dell'Isola, F.; Esposito, R.; Pulvirenti, M.: Macroscopic description of microscopically strongly inhomogenous systems: A mathematical basis for the synthesis of higher gradients metamaterials. *Archive for Rational Mechanics and Analysis*, 218, (2015), 1239–1262.

Cazzani, A.; Malagù, M.; Turco, E.: Isogeometric analysis of plane-curved beams. *Mathematics and Mechanics of Solids*, 21, 5, (2016a), 562–577.

Cazzani, A.; Malagù, M.; Turco, E.; Stochino, F.: Constitutive models for strongly curved beams in the frame of isogeometric analysis. *Mathematics and Mechanics of Solids*, 21, 2, (2016b), 182–209.

Cuomo, M.; dell'Isola, F.; Greco, L.: Simplified analysis of a generalized bias-test for fabrics with two families of inextensible fibres. *Zamp - Zeitschrift für angewandte Mathematik und Physik*, 67, 3, (2016), 61. DOI: 10.1007/s00033–016–0653–z.

Del Vescovo, D.; Giorgio, I.: Dynamic problems for metamaterials: review of existing models and ideas for further research. *International Journal of Engineering Science*, 80, (2014), 153–172.

dell'Isola, F.; Cuomo, M.; Greco, L.; Della Corte, A.: Bias extension test for pantographic sheets: numerical simulations based on second gradient shear energies. *Journal of Engineering Mathematics*, pages 1–31. doi:10.1007/s10665–016–9865–7.

dell'Isola, F.; D'Agostino, M. V.; Madeo, A.; Boisse, P.; Steigmann, D.: Minimization of shear energy in two dimensional continua with two orthogonal families of inextensible fibers: The case of standard bias extension test. *Journal of Elasticity*, 122, 2, (2016b), 131–155.

dell'Isola, F.; Della Corte, A.; Greco, L.; Luongo, A.: Plane bias extension test for a continuum with two inextensible families of fibers: A variational treatment with lagrange multipliers and a perturbation solution. *International Journal of Solids and Structures*, 81, (2016c), 1–12.

dell'Isola, F.; Giorgio, I.; Pawlikowski, M.; Rizzi, N. L.: Large deformations of planar extensible beams and pantographic lattices: heuristic homogenization, experimental and numerical examples of equilibrium. In: *Proc. R. Soc. A*, vol. 472, page 20150790, The Royal Society (2016d).

dell'Isola, F.; Lekszycki, T.; Pawlikowski, M.; Grygoruk, R.; Greco, L.: Designing a light fabric metamaterial being highly macroscopically tough under directional extension: first experimental evidence. *Zeitschrift für angewandte Mathematik und Physik*, 66, 6, (2015a), 3473–3498.

dell'Isola, F.; Madeo, A.; Seppecher, P.: Cauchy tetrahedron argument applied to higher contact interactions. *Archive for Rational Mechanics and Analysis*, 219, 3, (2016e), 1305–1341.

dell'Isola, F.; Sciarra, G.; Vidoli, S.: Generalized hooke's law for isotropic second gradient materials. In: *Proceedings of the Royal Society of London A: Mathematical, Physical and Engineering Sciences*, pages rspa–2008, The Royal Society (2009).

dell'Isola, F.; Seppecher, P.; Della Corte, A.: The postulations á la D'Alembert and á la Cauchy for higher gradient continuum theories are equivalent: a review of existing results. *Proceedings of the Royal Society of London A*, 471, 2183, (2015b), 20150415.

dell'Isola, F.; Seppecher, P.; Madeo, A.: Beyond Euler-Cauchy continua: The structure of contact actions in N-th gradient generalized continua: a generalization of the Cauchy tetrahedron argument. In: *Variational Models and Methods in Solid and Fluid Mechanics*, pages 17–106, Springer (2011).

dell'Isola, F.; Steigmann, D.; Della Corte, A.: Synthesis of fibrous complex structures: Designing microstructure to deliver targeted macroscale response. *Applied Mechanics Reviews*, 67, 6, (2015c), 060804.

Enakoutsa, K.; Della Corte, A.; Giorgio, I.: A model for elastic flexoelectric materials including strain gradient effects. *Mathematics and Mechanics of Solids*, 21, 2, (2016), 242–254.

Eremeyev, V. A.; Lebedev, L. P.: Mathematical study of boundary-value problems within the framework of Steigmann–Ogden model of surface elasticity. *Continuum Mechanics and Thermodynamics*, 28, 1-2, (2016), 407–422.

Ferretti, M.; Madeo, A.; dell'Isola, F.; Boisse, P.: Modeling the onset of shear boundary layers in fibrous composite reinforcements by second-gradient theory. *Zeitschrift für angewandte Mathematik und Physik*, 65, 3, (2014), 587–612.

Germain, P.: The method of virtual power in continuum mechanics. Part 2: Microstructure. *SIAM J. Appl. Math.*, 25, 3, (1973), 556–575.

Giorgio, I.: Numerical identification procedure between a micro-Cauchy model and a macro-second gradient model for planar pantographic structures. *ZAMP - Zeitschrift für angewandte Mathematik und Physik*, 67, 4, (2016), 95. doi:10.1007/s00033–016–0692–5.

Giorgio, I.; Della Corte, A.; dell'Isola, F.; Steigmann, D. J.: Buckling modes in pantographic lattices. *Comptes rendus Mécanique*, 344, 7, (2016), 487–501.

Giorgio, I.; Galantucci, L.; Della Corte, A.; Del Vescovo, D.: Piezo-electromechanical smart materials with distributed arrays of piezoelectric transducers: current and upcoming applications. *International Journal of Applied Electromagnetics and Mechanics*, 47, 4, (2015), 1051–1084.

Giorgio, I.; Scerrato, D.: Multi-scale concrete model with rate-dependent internal friction. *European Journal of Environmental and Civil Engineering*, DOI:10.1080/19648189.2016.1144539, (2016), 19.

Greco, L.; Cuomo, M.: Consistent tangent operator for an exact Kirchhoff rod model. *Continuum Mechanics and Thermodynamics*, 27, 4, (2015), 861–877.

Greco, L.; Cuomo, M.: An isogeometric implicit G1 mixed finite element for Kirchhoff space rods. *Comput Methods Appl Mech Eng*, 298, (2016), 325–349.

Harrison, P.: Normalisation of biaxial bias extension test results considering shear tension coupling. *Composites Part A: Applied Science and Manufacturing*, 43, 9, (2012), 1546–1554.

Harrison, P.: Modelling the forming mechanics of engineering fabrics using a mutually constrained pantographic beam and membrane mesh. *Composites Part A: Applied Science and Manufacturing*, 81, (2016), 145–157.

Harrison, P.; Abdiwi, F.; Guo, Z.; Potluri, P.; Yu, W. R.: Characterising the shear–tension coupling and wrinkling behaviour of woven engineering fabrics. *Composites Part A: Applied Science and Manufacturing*, 43, 6, (2012), 903–914.

Harrison, P.; Clifford, M.; Long, A.: Shear characterisation of viscous woven textile composites: a comparison between picture frame and bias extension experiments. *Composites Science and Technology*, 64, 10, (2004), 1453–1465.

Harrison, P.; Potluri, P.: Shear tension coupling in biaxial bias extension tests (2009).

Luongo, A.; Zulli, D.: *Mathematical models of beams and cables*. John Wiley & Sons (2013).

Madeo, A.; Della Corte, A.; Greco, L.; Neff, P.: Wave propagation in pantographic 2D lattices with internal discontinuities. *Proceedings of the Estonian Academy of Sciences*, 64, 3S, (2015), 325–330.

Maurini, C.; Pouget, J.; Dell'Isola, F.: On a model of layered piezoelectric beams including transverse stress effect. *International journal of solids and structures*, 41, 16, (2004), 4473–4502.

Mindlin, R. D.: Micro-structure in linear elasticity. *Archive for Rational Mechanics and Analysis*, 16, 1, (1964), 51–78.

Nadler, B.; Steigmann, D. J.: A model for frictional slip in woven fabrics. *Comptes Rendus Mecanique*, 331, 12, (2003), 797–804.

Piccardo, G.; Ranzi, G.; Luongo, A.: A direct approach for the evaluation of the conventional modes within the gbt formulation. *Thin-Walled Structures*, 74, (2014), 133–145.

Pideri, C.; Seppecher, P.: A second gradient material resulting from the homogenization of an heterogeneous linear elastic medium. *Continuum Mechanics and Thermodynamics*, 9, 5, (1997), 241–257.

Placidi, L.; Andreaus, U.; Giorgio, I.: Identification of two-dimensional pantographic structure via a linear D4 orthotropic second gradient elastic model. *Journal of Engineering Mathematics*, DOI: 10.1007/s10665-016-9856-8.

Ranzi, G.; Luongo, A.: A new approach for thin-walled member analysis in the framework of gbt. *Thin-Walled Structures*, 49, 11, (2011), 1404–1414.

Scerrato, D.; Giorgio, I.; Della Corte, A.; Madeo, A.; Dowling, N.; Darve, F.: Towards the design of an enriched concrete with enhanced dissipation performances. *Cement and Concrete Research*, 84, (2016a), 48–61.

Scerrato, D.; Giorgio, I.; Della Corte, A.; Madeo, A.; Limam, A.: A micro-structural model for dissipation phenomena in the concrete. *International Journal for Numerical and Analytical Methods in Geomechanics*, 39, 18, (2015), 2037–2052.

Scerrato, D.; Giorgio, I.; Madeo, A.; Limam, A.; Darve, F.: A simple non-linear model for internal friction in modified concrete. *International Journal of Engineering Science*, 80, (2014), 136–152.

Scerrato, D.; Giorgio, I.; Rizzi, N. L.: Three-dimensional instabilities of pantographic sheets with parabolic lattices: numerical investigations. *Zeitschrift für angewandte Mathematik und Physik - ZAMP*, 67, 3, (2016b), 53. DOI:10.1007/s00033–016–0650–2.

Scerrato, D.; Zurba Eremeeva, I. A.; Lekszycki, T.; Rizzi, N. L.: On the effect of shear stiffness on the plane deformation of linear second gradient pantographic sheets. *ZAMM - Zeitschrift für Angewandte Mathematik und Mechanik*, 96, 11, (2016c), 1268–1279.

Shen, H.; Qiu, J.; Ji, H.; Zhu, K.; Balsi, M.; Giorgio, I.; dell'Isola, F.: A low-power circuit for piezoelectric vibration control by synchronized switching on voltage sources. *Sensors and actuators A: Physical*, 161, 1, (2010), 245–255.

Turco, E.; dell'Isola, F.; Rizzi, N. L.; Grygoruk, R.; Müller, W. H.; Liebold, C.: Fiber rupture in sheared planar pantographic sheets: Numerical and experimental evidence. *Mechanics Research Communications*, 76, (2016), 86–90.

Address: Antonio Battista, Laboratoire des Sciences de l'Ingénieur pour l'Environnement,
Université de La Rochelle, France
Avenue Michel Crépeau
17042 La Rochelle cedex 1
email: antonio.battista@univ-lr.fr

Address: Dionisio Del Vescovo, Dipartimento di Ingegneria Meccanica e Aerospaziale
Sapienza, Università di Roma
Via Eudossiana, 18 - 00184 ROMA
email: dinonisio.delvescovo@uniroma1.it

Address: Nicola Luigi Rizzi, Università degli Studi Roma Tre
Dipartimento di Architettura
via della Madonna de' Monti, 40
00184 Roma
email: nicolaluigi.rizzi@uniroma3.it

Address: Emilio Turco, University of Sassari
Department of Architecture, Design and Urban planning
via Garibaldi 35, Asilo Sella
07041 Alghero (SS)
email: emilio.turco@uniss.it